Dielectrophoretic Manipulation of Cells with Spiral Electrodes

Xiao-Bo Wang, Ying Huang, Xujing Wang, Frederick F. Becker, and Peter R. C. Gascoyne
Department of Experimental Pathology, University of Texas M. D. Anderson Cancer Center, Houston, Texas 77030 USA

ABSTRACT Electrokinetic responses of human breast cancer MDA-MB-231 cells were studied in suspensions of conductivities 18, 56, and 160 mS/m on a microelectrode array consisting of four parallel spiral electrode elements energized with phase-quadrature signals of frequencies between 100 Hz and 100 MHz. At low frequencies cells were levitated and transported toward or away from the center of the spiral array, whereas at high frequencies cells were trapped at electrode edges. The frequencies of transition between these characteristic cell behaviors increased with increasing suspension conductivity. Levitation heights and radial velocities were determined simultaneously for individual cells as a function of the applied field magnitude and frequency. Results were compared with theoretical predictions from generalized dielectrophoresis theory applied in conjunction with cell dielectric parameters and simulated electric field distributions corrected for electrode polarization effects. It was shown that the conventional and traveling-wave dielectrophoretic force components dominated cell levitation and radial motion, respectively. Both theoretical predictions and experimental data showed that the cell radial velocity was very sensitive to the field frequency when the in-phase component of the field-induced polarization was close to zero. Applications of spiral electrode arrays, including the isolation of cells of clinical relevance, are discussed.

INTRODUCTION

The ability to selectively manipulate living cells in three dimensions according to specific cell properties is fundamental to many biological and medical applications. For example, the sensitive detection and isolation of malignant cells from peripheral blood and bone marrow is critical for the diagnosis of cancer, for monitoring residual disease during and after chemotherapy, and for early determination of relapse after remission (Chan et al., 1994; Craig et al., 1992; Gross et al., 1995). Forces that can be used for cell manipulation include those of mechanical, optical, electromagnetic, and ultrasonic origins. Successful examples of the use of these forces include cell sorting and characterization by flow cytometry (Ormerod, 1994), cell manipulation with laser tweezers (Kuo and Sheetz, 1993), and cell separation with antibody-labeled magnetic beads (Bertoncello et al., 1991).

Dielectrophoresis (DEP), particle motion caused by the interaction between nonuniform A.C. electric fields and field-induced polarizations in particles, is currently receiving considerable interest because it enables noninvasive, electrical manipulations of cells (Gascoyne et al., 1992; Kaler et al., 1992; Masuda et al., 1987; Fuhr et al., 1995; Wang et al., 1995). Two basic types of DEP force exist: conventional DEP (cDEP) in a field of nonuniform strength, and traveling-wave DEP (twDEP) in a traveling electrical field. DEP manipulation has been demonstrated in examples of cell collection in strong or weak field regions (Gascoyne et al., 1992; Wang et al., 1993), trapping in so-called three-dimensional field cages (Fuhr et al., 1992), levitation against gravity (Kaler et al., 1992), and linear transportation in traveling electric fields (Masuda et al., 1987; Huang et al., 1993; Fuhr et al., 1995; Wang et al., 1995). Because of the sensitive dependence of DEP responses on cell dielectric properties, separation of cells possessing different dielectric properties is possible and has been demonstrated using the approaches of cDEP migration (Gascoyne et al., 1992; Wang et al., 1993; Markx et al., 1994) and cDEP retention (Becker et al., 1994, 1995; Talary et al., 1995). For example, we have recently achieved the removal of human breast cancer cells and leukemia cells from dilute human blood in a dielectrophoretic affinity column in which a competition between hydrodynamic and cDEP forces is exploited (Becker et al., 1994, 1995). Furthermore, using cDEP and twDEP forces, Talary et al. (1996) have recently demonstrated the separation of viable from nonviable yeast cells using a traveling electrical field.

Here we report the design and characterization of a concentric spiral electrode system. When operated under appropriate conditions, target cell types from a cell mixture may be selectively moved to either the center or periphery of the array. By studying the electrokinetic responses of human breast cancer MDA-MB-231 cells, we demonstrate that spiral arrays can generate cDEP and twDEP forces, causing cell entrapment, levitation, and radial motion. We provide simultaneous measurements of cell radial velocities and levitation heights as a function of the frequency and/or amplitude of the applied voltage signals. These data are analyzed in terms of the generalized DEP theory in conjunction with the electrical field distributions, electrode polarization effects, and cell dielectric properties. This analysis reveals the dependency of cell kinetic behavior on the in-phase and out-of-phase components of field-induced polarizations. It is shown that cells are trapped or levitated

Received for publication 30 September 1996 and in final form 10 January 1997.

Address reprint requests to Dr. Xiao-Bo Wang, Department of Experimental Pathology, Box 89, University of Texas MD Anderson Cancer Center, 1515 Holcombe Boulevard, Houston, TX 77030. Tel.: 713-792-7605; Fax: 713-792-5940; E-mail: xiaobo@odin.mdacc.tmc.edu.

0006-3495/97/04/1887/13 $2.00

mainly by cDEP forces, and when levitated, cells are then caused to move in a radial direction by twDEP forces. Because the strength of the traveling field depends on the height above the electrode plane, the radial cell velocity is also height- and, therefore, cDEP force-dependent. Potential applications of the spiral electrode array for cell concentration, manipulation, and separation are discussed in the context of previously reported electrode structures.

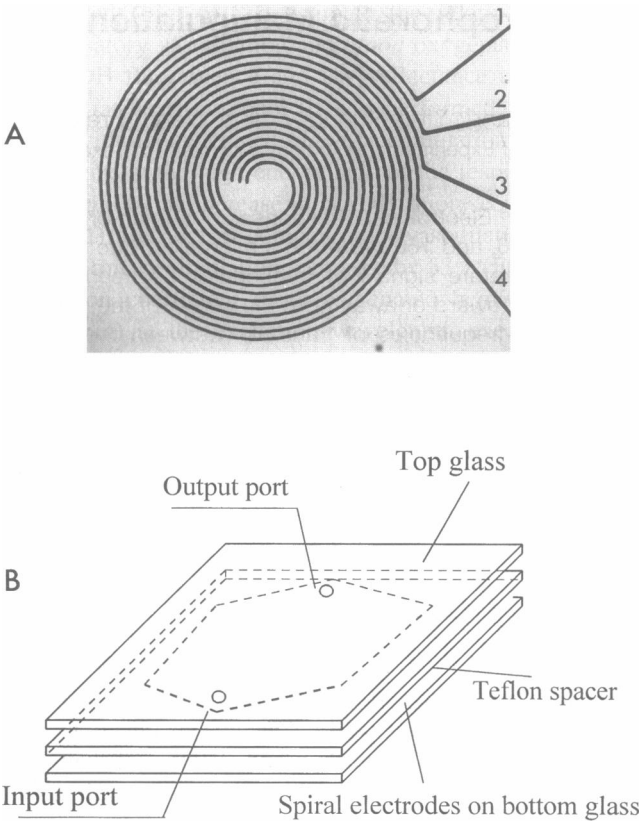

FIGURE 1 (*A*) A spiral electrode array. We define the condition that electrodes 1, 2, 3, and 4 are energized with voltage signals of phase 0°, 90°, 180°, and 270°, respectively, as the outward-excitation sequence. Reversal of this phasing results in the inward-excitation sequence. (*B*) Schematic representation of the electromanipulation chamber containing a spiral electrode array.

MATERIALS AND METHODS

Cell preparation

The human breast cancer cell line, MDA-MB-231, originally derived from a pleural effusion of a patient with metastatic breast carcinoma (Zhang et al., 1991), was chosen as the model cell type in this study because we planned to investigate the possibility of isolating breast cancer cells from normal cell mixtures. Cells were cultured in minimum essential/F12 medium supplemented with 10% fetal bovine serum, 1 mM glutamine, and 20 mM HEPES (Gibco), 0.5% penicillin, and streptomycin solution (Sigma). The cultures were maintained in 75-cm^2 plastic flasks in 5% CO_2/95% air at 37°C in a humidified incubator. The cells were harvested at ~80% confluence 48 h after seeding by 3-min exposure of the monolayer to 0.25% trypsin–0.02% EDTA solution. Cells were dislodged by tapping the flask, and then suspended in serum-supplemented medium to neutralize the trypsin. Cell suspensions were found to have >95% viability, as determined by Trypan blue dye exclusion. Harvested cells in complete culture medium were diluted to approximately 5×10^4/ml with isotonic 8.5% (w/v) sucrose plus 0.3% (w/v) dextrose buffer. The conductivities of the final suspensions in different samples were adjusted with culture medium to be 18, 56, and 160 mS/m, respectively, as determined with a conductivity meter (EC19101-00; Cole-Parmer Instruments). To quantify cell sedimentation effects, the specific density of MDA-MB-231 cells was assessed to be 1.074 g/cm^3 by using centrifugally generated continuous Percoll density gradients (Pharmacia) calibrated with Percoll density marker beads. The specific density of the cell suspending medium was determined to be 1.033 g/cm^3 with a hydrometer (VWR Scientific).

Electrode fabrication

Spiral microelectrode arrays, shown in Fig. 1, were fabricated using standard photolithography. In brief, gold-coated (thickness 250 Å over a 100-Å chrome seeding layer) glass blanks (25 mm × 25 mm; Thin Film Technology) were spin-coated at 3000 rpm with S1830 photoresist (Shipley) to ~1 μm thickness. Here the spin rate and resist viscosity determined the spreading and consequently the final thickness of coated photoresist. The photoresist was polymerized by baking on a hotplate at 110°C for 1 min, and then exposed to UV light through a positive image (Laser CAD) of the electrode array, using a mask aligner (HTG System 3A). The exposed photoresist was developed with MF351 developer, and the corresponding gold and chrome region was then etched. Finally, the remaining layer of the photoresist on the electrodes was removed with acetone. Equal electrode widths and gaps of 20 μm were chosen to accommodate the size of the breast cancer cells (average 12 μm diameter) to ensure that they were subjected to a continuously traveling electric field.

Cell manipulation

The cell manipulation chamber, shown in Fig. 1, was constructed of glass top and bottom walls separated by a 250-μm-thick Teflon spacer. The bottom glass wall had on its inner surface the spiral electrode array. Plastic tubes of diameter 1.22 mm glued into holes drilled through the top glass wall allowed for the introduction and withdrawal of cell suspensions. After introduction of a sample, cells were allowed to settle for about 10 s onto the electrode plane before the application of electrical signals. Phase-quadrature sinusoidal voltages between 1 kHz and 100 MHz and up to 1 V RMS from a custom-built signal generator (Hölzel, 1993) were connected to the four electrode elements in sequence through 50-Ω coaxial cables. A two-way, two-pole switch was used to conveniently reverse the phase sequence. The magnitude and phase relationship of the voltage signals were checked with a Tektronix 7904A oscilloscope (7B10; 2-ns time base). Cell electrokinetic behaviors were viewed through a Nikon TMD inverted microscope equipped with a Hamamatsu CCD video camera and recorded on videotape. Objective lenses of 4× to 40× provided final magnifications between 140× to 1400× on the TV monitor. For cell levitation experiments, the height of cells above the electrode plane was measured to an accuracy of ±2 μm by focusing first on the electrode plane and then on the cells and subtracting the corresponding readings on the focusing dial. Cell radial velocity was determined by measuring the time taken for individual cells to move at least 80 μm. Lateral distances were calibrated using a stage micrometer. To quantify the cell behavior, levitation heights and radial velocities were determined simultaneously for at least 12 individual cells as a function of the applied field frequency and voltage at each suspension conductivity.

Determination of electrode polarization effects

When voltage signals were applied to the spiral electrode array, a portion of the voltage was dropped across the electrode/solution interface because of the interfacial impedance. Thus the voltage applied to the bulk suspending medium was smaller than that on the electrodes. To quantify this

so-called electrode polarization (Schwan, 1992) for accurate calculation of DEP forces, we measured the frequency dependencies of the voltages on the spiral electrodes for a signal generator having a specified source voltage and impedance. In this way, the source voltage was effectively divided between the source impedance, the electrode/solution interface, and the bulk suspending medium. By applying several commonly used electrode polarization models (Schwan, 1992), an optimization procedure was used to calculate the impedances due to the electrode polarization and the bulk solution (see later).

DEP force analysis

To better understand the observed cell kinetic behaviors, DEP forces were simulated based on cell dielectric parameters and the electrical field distribution for spiral electrodes. MDA-MB-231 cell dielectric properties were determined using electrorotation (ROT) measurements (Huang et al., 1995) on polynomial electrodes.

The electric field simulations of the spiral electrode array were performed on a Sparc 20 workstation in a C program using the Greens'-theorem-based method (Wang et al., 1996). For simplicity, the spiral electrode array was approximated as a number of concentric, circular electrode elements energized by voltage signals shifted in phase by $\pi/2$ between adjacent elements. The spatial distributions of the magnitude and phase of each electrical field component were obtained through integral calculations of the known boundary conditions of the electrical potentials across the electrode plane (Wang et al., 1996). The theoretical DEP forces containing both cDEP and twDEP components were then determined using the generalized DEP theory (Wang et al., 1995).

RESULTS

Overall electrokinetic effects

The electrokinetic responses of MDA-MB-231 cells on the spiral electrodes are summarized in Fig. 2. Cells exhibited the following characteristic behaviors in sequential order as the applied field frequency was increased: levitation and cofield radial motion; levitation and antifield radial motion; transitional behavior; and entrapment at the edges of the electrode elements. With increasing suspension conductivity, the frequency regions for these behaviors shifted to higher frequencies (Fig. 2). By switching the voltage signals applied to the electrode array from phase quadrature to phase opposition, it was observed that, just as in the case of cell kinetic behaviors in a traveling electric field (Huang et al., 1993), the regime of cell entrapment coincided with the frequency ranges in which positive cDEP (particles being directed toward the strong electrical field regions) was operative.

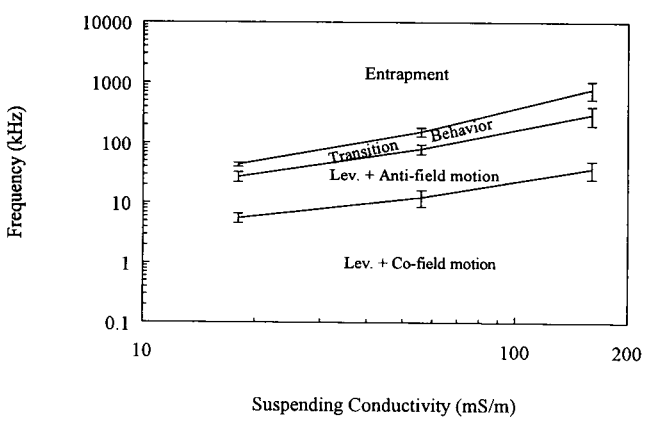

FIGURE 2 Electrokinetic responses of MDA-MB-231 cells on a spiral electrode array. Error bars indicate standard deviations of the cell cross-over frequencies between different characteristic behaviors. Numbers of cells characterized were 12, 14, and 13 for suspension conductivities of 18, 56, and 160 mS/m, respectively.

To further elucidate these effects, we examined the cell behaviors in detail for the suspension conductivity of 56 mS/m. For clarity we here define voltage signals of phase 0°, 90°, 180°, and 270° connected, respectively, to electrode elements 1–4 in Fig. 1 as the outward-excitation sequence (because the electrical potential wave then travels toward the periphery of the spiral array) and voltage signals of reversed phase order as the inward-excitation sequence.

Levitation and cofield motion

Voltage signals between 0.5 and ~10 kHz levitated cells above the electrode plane in several seconds to characteristic equilibrium positions, where they exhibited radial motion toward or away from the center of the spiral electrode array for the inward- and outward-excitation sequences, respectively. The levitation process was clearly demonstrated by observing the gradual loss of focus on cells under microscopy. For an applied RMS voltage of 0.7 V, the typical cell levitation height increased from ~20 μm at 0.5 kHz to ~50 μm at 10 kHz. The cell radial velocity was ~1 μm/s in the cofield direction and appeared to be similar for all cells.

Levitation and antifield motion

Voltage signals between ~10 and ~75 kHz levitated cells and moved them toward or away from the center of the spiral array for the outward- or inward-excitation sequence, respectively (Fig. 3) (i.e., cells underwent radial motions in the direction opposite to that of the applied traveling electrical waves). The instantaneous radial velocity of individual cells remained almost constant during their radial motion until they reached either the center or the periphery of the electrode array. The kinetic behavior of cells was independent of their initial positions on the spiral electrode. Furthermore, each cell exhibited rotation about an axis through its center that was oriented parallel to the electrode plane and normal to the radial direction. Individual cells differed greatly in their kinetic behavior. For example, for a given excitation, cell heights differed by as much as 30 μm (corresponding to a relative difference of about 150%), and fast-moving cells traveled up to 5 times faster then slow ones.

Transitional behavior

Voltage signals between ~75 and ~140 kHz produced a transition in cell behavior from radial motion to entrapment. In this frequency range, radial motions toward either the

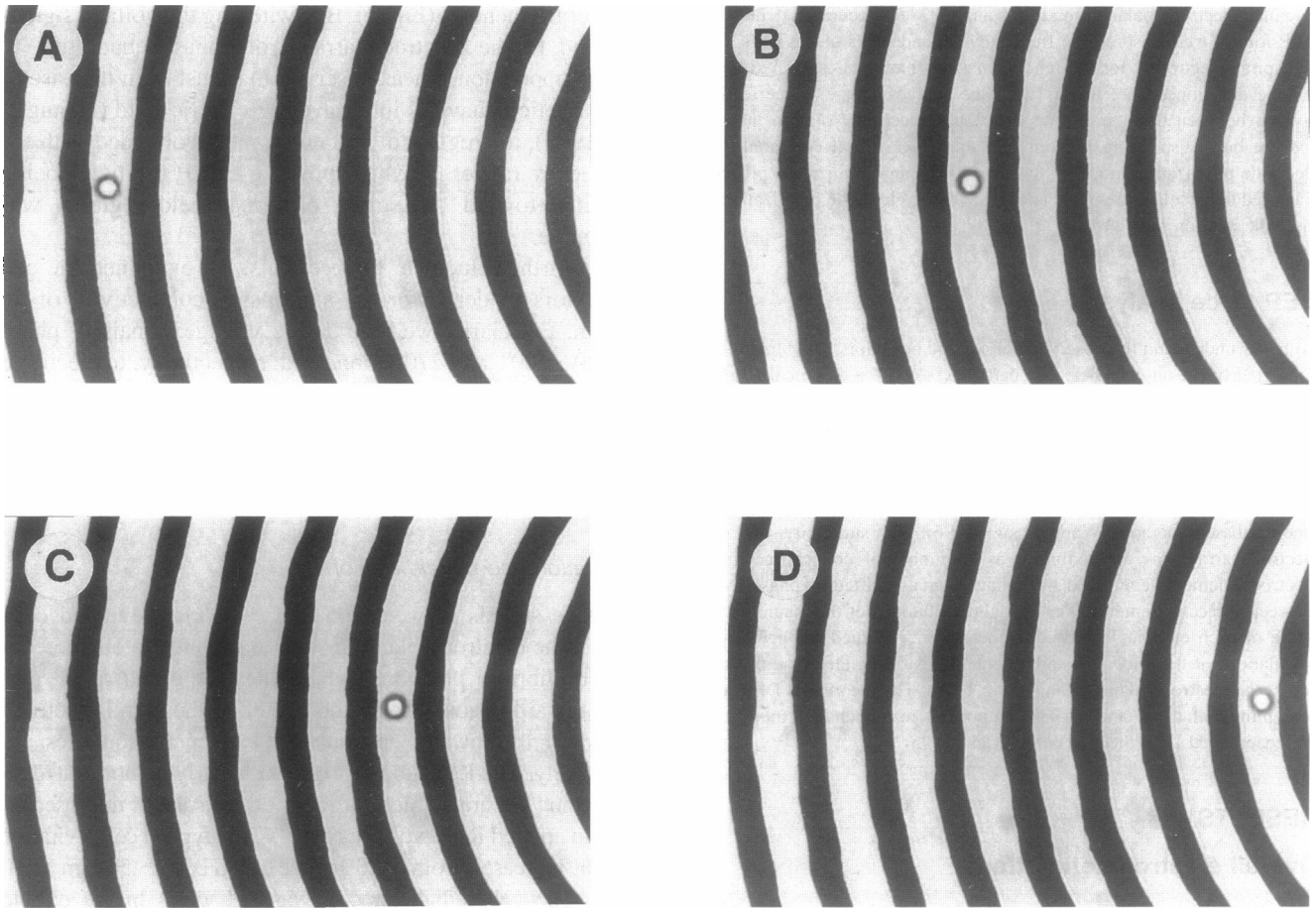

FIGURE 3 A portion of a spiral electrode array showing an MDA-MB-231 cell being directed to the center by an outward phase excitation of 40 kHz and 0.7 V RMS. The cell was levitated above the electrode plane, as evidenced by the fact that it appears out of focus. The time interval between each consecutive photograph (*A–D*) was about 4 s, indicating an average cell velocity of 20 μm/s.

center or periphery of the electrode array were observed for different cells simultaneously. The cell instantaneous velocities varied, depending on their position relative to the electrode elements, as evidenced by unsteady radial movement. Still other cells were loosely trapped at the electrode edges, exhibiting fast rotation.

Entrapment

Upon application of voltage signals between ~140 kHz and 100 MHz, cells were quickly attracted to electrode edges and trapped there, exhibiting little or no rotation. Under the inward-excitation sequence, cell trapping occurred preferentially at the outward-facing and the inward-facing edges of the electrode elements in the frequency ranges ~140 to ~500 kHz and ~40 to 100 MHz, respectively (Fig. 4).

Levitation height and radial velocity of individual cells

To quantify cell behavior, we determined simultaneously both the levitation height and radial velocity of individual cells as a function of the frequency and magnitude of the applied voltage signals. The frequency dependencies for three individual cells are shown in Fig. 5 for suspension conductivities of 18, 56, and 160 mS/m, respectively. We will take the case of the particular cell in the suspension conductivity of 56 mS/m as an example for discussion. As the frequency was varied from 100 Hz to 20 kHz, the cell height increased steadily from ~22 to ~55 μm, and the cell radial motion changed from a cofield velocity of ~1.5 μm/s to an antifield velocity of ~0.5 μm/s. As frequency increased further to 60 kHz, the cell height exhibited a sharp decrease to ~15 μm, and antifield velocity increased rapidly to ~40 μm/s. Within the narrow band from 65 to 75 kHz, the cell height fell further to ~10 μm, and the cell could not cross the electrode gaps and was trapped between the electrode elements. However, in the higher frequency band from 85 to 120 kHz, the cell exhibited cofield radial motion at velocities as high as 28 μm/s. At frequencies above 120 kHz, motion ceased and the cell was trapped at the electrode edges.

Fig. 6 shows the voltage dependencies of levitation height and radial velocity for three individual MDA-MB-231 cells at fixed applied field frequencies for suspension conductivities of 18, 56, and 160 mS/m, respectively. We

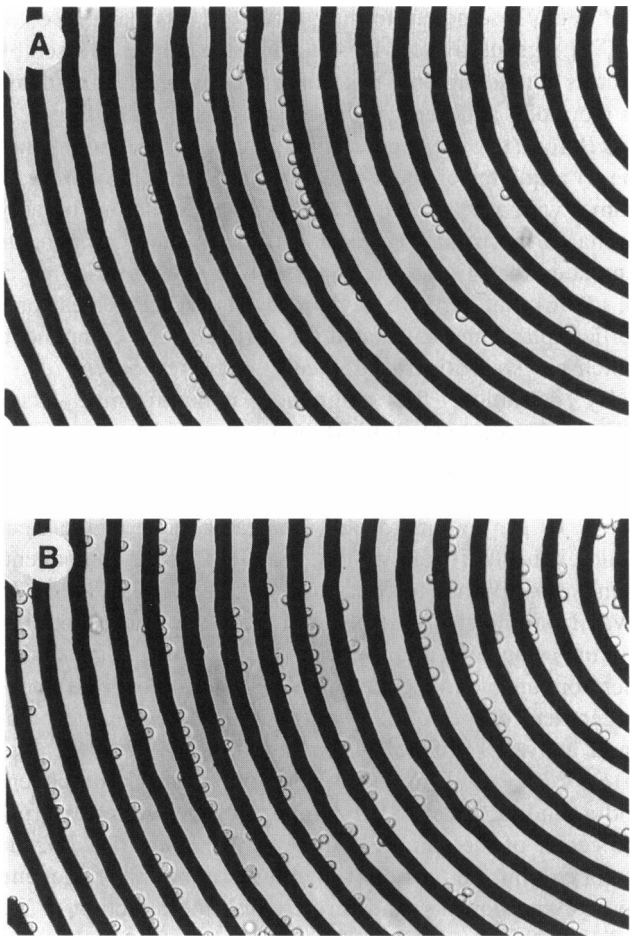

FIGURE 4 MDA-MB-231 cells trapped at electrode edges under phase quadrature voltage excitation at 300 kHz and 0.7 V RMS. (*A*) Cells were collected at outward-facing edges of the electrode elements under inward-phase excitation. (*B*) Cells were collected at inward-facing electrodes under outward-phase excitation.

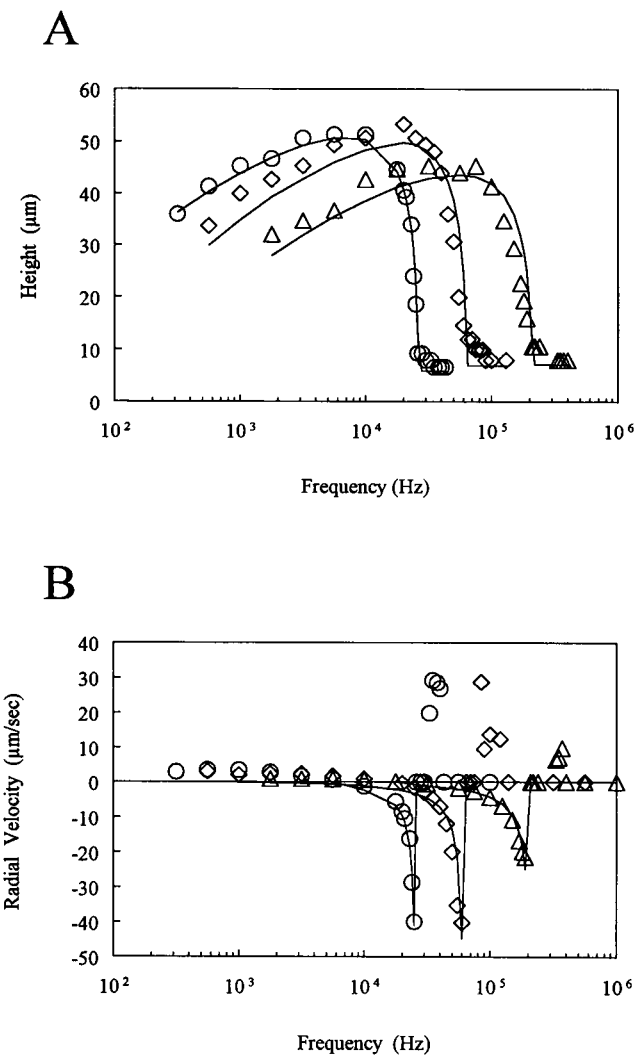

FIGURE 5 Frequency dependencies of (*A*) heights above the electrode plane and (*B*) radial velocities of three MDA-MB-231 cells in suspensions of conductivity 18 (○, radius $r = 5.94$ μm), 56 (◇, $r = 6.93$ μm) and 160 (△, $r = 7.11$ μm) mS/m. Continuous curves represent the best-fit theoretical dependencies calculated according to Eqs. 3 and 6. Membrane-specific capacitance and conductance values were derived using an optimized single-shell dielectric model. Because of the field complexity at positions close to the electrode plane, cell radial velocity was taken to be zero for heights below 12 μm. Electrode polarization effects, as shown in Fig. 9, were taken into account in the theoretical simulation to correct the effective applied voltage.

will again consider the case of conductivity 56 mS/m at a field frequency of 80 kHz. As the applied voltage increased from 0 to 0.9 V, the levitation height increased monotonically up to 37 μm. For the same voltage range, cell radial velocity did not obey the square-voltage dependence, as observed for cell ROT (Huang et al., 1992), cDEP (Kaler et al., 1992), or linear twDEP effects (Huang et al., 1993). Instead, a sublinear dependency of velocity on the applied voltage was observed. For voltages of 0.25 V and below, cell motion did not occur, whereas above 0.3 V, cell velocity increased with voltage until it reached a plateau at ~0.6 V, remaining nearly constant with further increases in voltage.

DISCUSSION

DEP force analysis

The dielectrophoretic force acting on a cell of radius r as the result of an applied AC field of frequency ω, according to the effective dipole moment approach, is given by (Wang et al., 1995)

$$\vec{F} = 2\pi\varepsilon_m r^3[\mathrm{Re}(f_{CM})\nabla E_{RMS}^2 + \mathrm{Im}(f_{CM})(E_{x0}^2\nabla\varphi_x + E_{y0}^2\nabla\varphi_y + E_{z0}^2\nabla\varphi_z)], \quad (1)$$

where E_{RMS} is the RMS value of the field strength, $E_{\alpha 0}$ and φ_α ($\alpha = x, y, z$) are the magnitude and phase of each field component in a Cartesian coordinate frame, and $\mathrm{Re}(f_{CM})$ and $\mathrm{Im}(f_{CM})$ are the real (in-phase) and imaginary (out-of-phase) components of the Clausius-Mossotti factor f_{CM},

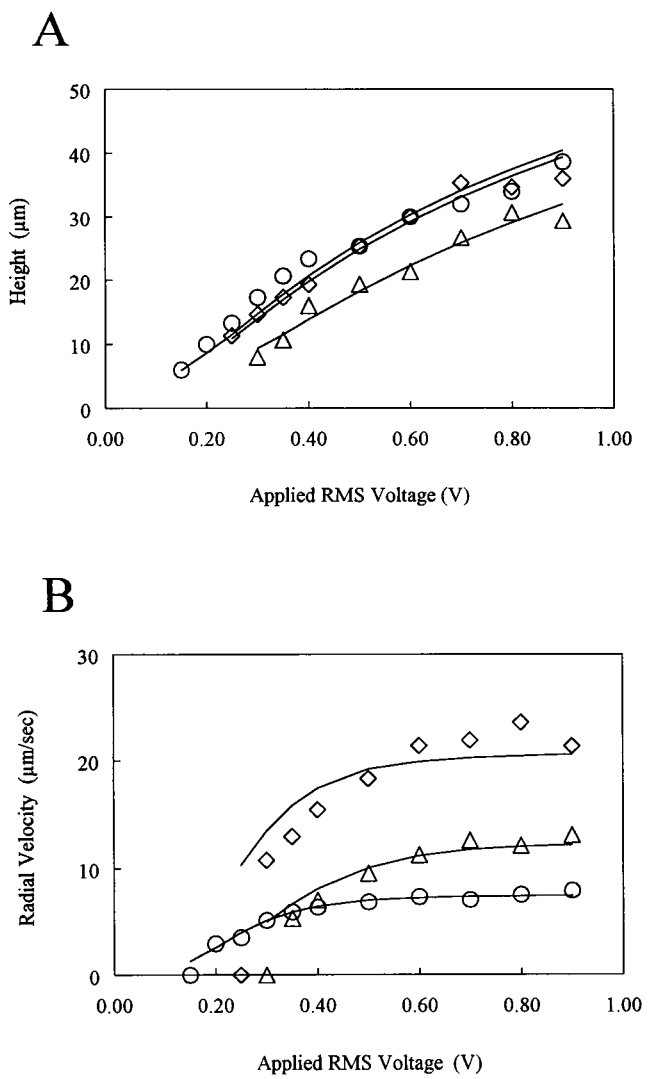

FIGURE 6 Voltage dependencies of (*A*) heights and (*B*) radial velocities of three MDA-MB-231 cells in suspensions of conductivity 18 (○, radius r = 5.94 μm), 56 (◇, r = 7.38 μm), and 160 (△, r = 6.12 μm) mS/m. Continuous curves represent the best-fit theoretical dependencies calculated using Eqs. 3 and 6. Because of the field complexity at positions close to the electrode plane, cell radial velocity was taken to be zero in the analysis for heights below 12 μm.

respectively. f_{CM} reflects the magnitude and direction of field-induced dipolar polarization in the cell, given by $f_{CM} = (\epsilon_c^* - \epsilon_m^*)/(\epsilon_c^* + 2\epsilon_m^*)$, where ϵ_c^* and ϵ_m^* are the complex dielectric permittivities of the cell and its surrounding medium. Thus the magnitude and phase distributions of field components, coupled with the frequency and suspension conductivity-dependent Clausius-Mossotti factor, determine the DEP forces experienced by a cell.

As described earlier, a concentric ring model was used for the analysis of the spiral electrode array. For this reason, the electrical field was independent of the angular direction of the spiral and dependent only on the radial distance from the electrode center and the height above the electrode plane. In this case, the field magnitude nonuniformity factor ∇E_{RMS}^2 and field phase nonuniformity factor $(E_{x0}^2\nabla\varphi_x + E_{y0}^2\nabla\varphi_y + E_{z0}^2\nabla\varphi_z)$, generally of 3-D vector form, can be expressed by vectors containing only two nonzero components orientated in the radial and vertical directions, as shown in Fig. 7, *A* and *B*, for a chosen angular direction of $\theta = 0$ (corresponding to a quarter of the x-z plane in a Cartesian coordinate frame, with $x > 0$ and $z > 0$). These results are broadly similar to horizontal cDEP and twDEP force components simulated for a linear electrode array reported by Hughes et al. (1996), but here we have determined DEP forces for a vertical plane and calculated the vertical force component, which plays a critical role in cell kinetic responses.

By definition, the magnitude nonuniformity factor ∇E_{RMS}^2 always points toward the strong field regions. Thus its vertical component points to the electrode plane and its radial component, having appreciable values only at height below 10 μm, points toward the nearest edge of the electrode elements. It follows that the cDEP force component, being proportional to ∇E_{RMS}^2, can direct cells toward or away from the electrode plane in the vertical direction, but can only trap cells at or between the electrode edges and is therefore unable to induce lateral cell motion over distances larger than one electrode width/gap period. On the other hand, above 10 μm the phase nonuniformity factor $(E_{x0}^2\nabla\varphi_x + E_{y0}^2\nabla\varphi_y + E_{z0}^2\nabla\varphi_z)$ has a negligible vertical component and a unidirectional radial component pointing away from the center of the spiral electrode array. Below 10 μm, the factor exhibits comparable magnitudes in both its radial and vertical components, and furthermore, the direction of the radial component becomes reversed, so that the field components travel in the direction opposite that of the applied traveling potential wave. It follows that the twDEP component, being proportional to $(E_{x0}^2\nabla\varphi_x + E_{y0}^2\nabla\varphi_y + E_{z0}^2\nabla\varphi_z)$, results mainly in cell motion along the radial direction toward or away from the electrode center at high levitation positions and induces complex cell behavior for levitation heights below 10 μm. The overall kinetic responses of cells on the spiral electrode array result from the combined effects of the cDEP and twDEP force components. Thus, when the cDEP force is negative, cells will be levitated above the electrode plane and simultaneously transported toward the electrode center or periphery by the twDEP force. On the other hand, a large, positive cDEP force can trap cells at the electrode edges, overcoming any twDEP force that is present.

Levitation

In the frequency range in which levitation occurs, the dielectrophoretic force in the vertical direction levitates cells against the sedimentation force. At the equilibrium levitation position, the DEP and sedimentation forces balance, so that the net force acting on the cells in the vertical direction is zero, and

$$-\frac{4}{3}\pi r^3(\rho_c - \rho_m)g + \vec{F}_{DEP}(z)\cdot\vec{a}_z = 0, \qquad (2)$$

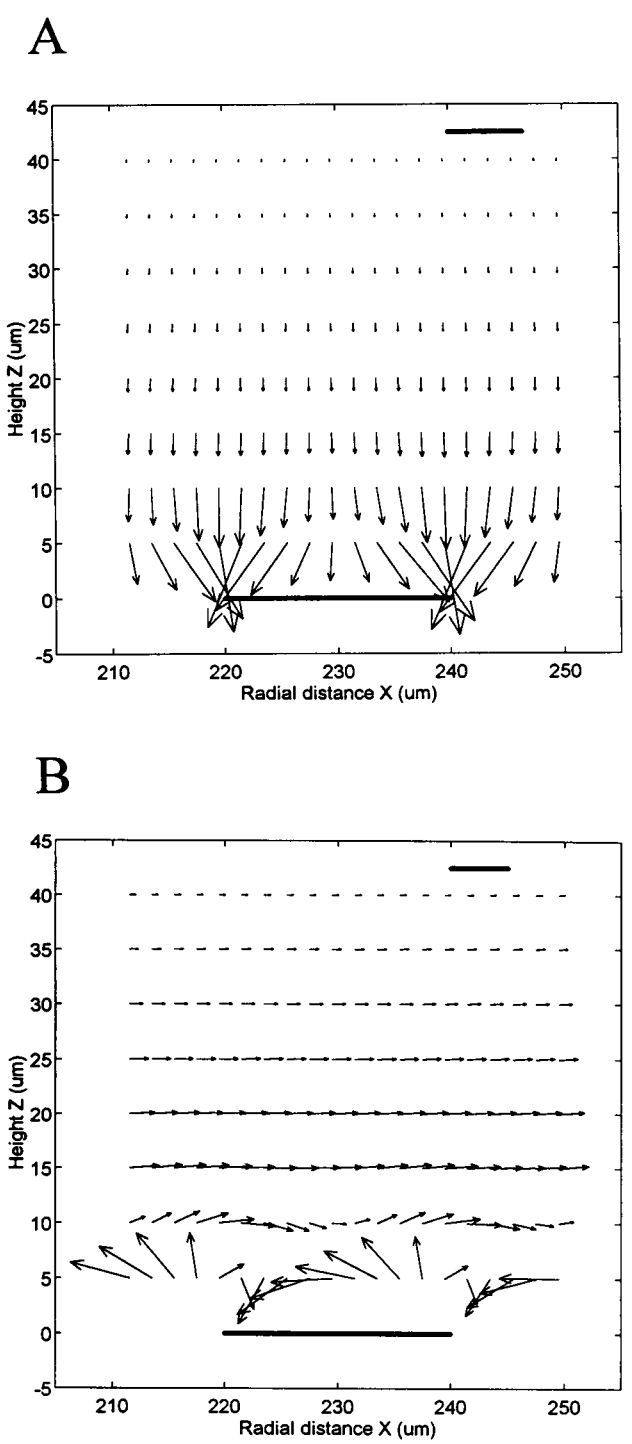

FIGURE 7 Vector representation of the distribution of (*A*) the field magnitude nonuniformity factor ∇E^2_{RMS} and (*B*) the field phase nonuniformity factor ($E^2_{x0}\nabla\varphi_x + E^2_{y0}\nabla\varphi_y + E^2_{z0}\nabla\varphi z$) produced by a spiral electrode array (width/gap = 20 μm) energized by phase-quadrature signals of 1 V (RMS). The electrode elements in the concentric ring model for the field simulation were located between the following radial coordinates: 60–80, 100–120, 140–160, 180–200, 220–240, 260–280, 300–320, and 340–360 μm. The electrode element at 220–240 μm is represented by the bold line on the *x* axis. Scale bar: (*A*) 2×10^{14} V^2/m^3; (*B*) 6×10^{13} V^2/m^3.

where ρ_c and ρ_m are the densities of the cell and the suspension medium, respectively. Because the twDEP force component in the vertical direction is almost zero for heights above 10 μm, Eq. 2 can be reduced to

$$2(\rho_c - \rho_m)g = 3\varepsilon_m \mathrm{Re}(f_{CM})\nabla E^2_{RMS}(z)\cdot\vec{a}_z \qquad (3a)$$

or

$$2(\rho_c - \rho_m)g = 3\varepsilon_m \mathrm{Re}(f_{CM})U^2\nabla E^2_0(z)\cdot\vec{a}_z, \qquad (3b)$$

where U is the applied voltage and $\nabla E^2_0 \cdot \vec{a}_z = \nabla E^2_{RMS}\cdot\vec{a}_z$ when $U = 1$ V. This reveals that the cell levitation is determined by the relative cell density ($\rho_c - \rho_m$), the cell dielectric property $\mathrm{Re}(f_{CM})$, the field distribution factor $\nabla E^2_0(z)\cdot\vec{a}_z$, and the applied voltage U. Several conclusions can be drawn by applying Eq. 3 to the cell measurements made in this study:

1. Because the specific density of MDA-MB-231 cells (1.074 g/cm^3) was larger than that (1.033 g/cm^3) of the suspending medium, negative cDEP forces occurring when $\mathrm{Re}(f_{CM}) < 0$ allowed for stable levitation of the cells.

2. As shown in Fig. 7 *A*, the factor $\nabla E^2_0(z)\cdot\vec{a}_z$ decreased monotonically with the distance z above the electrode plane. Thus, for the same applied voltage U, higher equilibrium positions are expected for cells with large values of $\mathrm{Re}(f_{CM})$.

3. To achieve levitation of a cell of radius r, the voltage U must be above the threshold value, $U_{th} = \sqrt{2(\rho_c - \rho_m)g/(3\epsilon_m \mathrm{Re}(f_{CM})\nabla E^2_{0|z=r}\cdot\vec{a}_z)}$. For MDA-MB-231 cells of typical radius 6 μm and a factor $\nabla E^2_{0|z=r}\cdot\vec{a}_z = -1.16 \times 10^{14}$ V^2/m^3, the threshold voltage is 82 mV when $\mathrm{Re}(f_{CM}) = -0.5$. Above U_{th}, cells are levitated to higher positions with increasing voltage and Eq. 3 holds. Fig. 6 *A* shows a comparison between experimental data and theoretical results for cell levitation at specified field frequencies as a function of the applied voltage. In deriving theoretical results, the value for $\mathrm{Re}(f_{CM})$ was optimized, so that a best fit of theory to experiment was achieved. The good agreement between theory and experiment shows the validity of modeling cell levitation using Eq. 3b.

As in the case of the cDEP levitation of single cells by a cone-plate electrode structure (Kaler and Jones, 1990), the levitation forces observed here arise predominately from the interaction of the field-induced dipolar polarization with the field nonuniformity factor ∇E^2_{RMS}. This is distinctly different from the case of DEP levitation at a field null, where DEP forces are induced by field-induced higher order polarization interacting with field higher order nonuniformity factors (see Fuhr et al., 1992, and the critique by Washizu et al., 1996).

Radial motion

The cell radial motion is determined by the radial components F_{DEPr} of DEP forces and the opposing Stokes' drag.

The corresponding electrokinetic equation is given by

$$\frac{4}{3}\pi r^3 \rho_c \frac{dV_r}{dt} = F_{DEPr} - 6\pi r\eta V_r, \quad (4)$$

where V_r is the cell velocity and η is the dynamic viscosity. For a typical cell of radius $r < 10$ μm and velocity $V_r < 100$ μm/s, the cell Reynolds number is <0.1. In such a heavily damped dynamic system, the instantaneous velocity is proportional to the applied instantaneous DEP force and is given by

$$\begin{aligned} V_r &= \frac{F_{DEPr}}{6\pi r\eta} \\ &= \frac{\varepsilon_m r^2}{3\eta}(\mathrm{Re}(f_{CM})\nabla E_{RMS}^2 \cdot \vec{a}_r + \mathrm{Im}(f_{CM}) \\ &\quad \cdot (E_{x0}^2\nabla\varphi_x + E_{y0}^2\nabla\varphi_y + E_{z0}^2\nabla\varphi_z)\cdot\vec{a}_r). \end{aligned} \quad (5)$$

Eq. 5 indicates

1. For cells of identical dielectric properties, large cells will move faster than small ones.

2. Both $\mathrm{Re}(f_{CM})$ and $\mathrm{Im}(f_{CM})$ contribute to the instantaneous cell radial velocity. Because the factor $\nabla E_{RMS}^2 \cdot \vec{a}_r$ varies with radial position, the instantaneous radial velocity alters with cell position, especially for cells at heights below 10 μm from the electrode surface (Fig. 7 *A*). However, because the factor $\nabla E_{RMS}^2 \cdot \vec{a}_r$ was found in field simulations to average to zero over each complete electrode-gap period, the cDEP force term does not affect the average cell velocity taken over one or more electrode-gap periods.

3. Because the factor $(E_{x0}^2\nabla\varphi_x + E_{y0}^2\nabla\varphi_y + E_{z0}^2\nabla\varphi_z)\cdot\vec{a}_r$ is strongly dependent on the cell height above the electrode plane (Fig. 7 *B*), the average radial velocity is very sensitive to the equilibrium levitation position, which in turn depends on the vertical cDEP force component (Eq. 3b). Thus $\mathrm{Re}(f_{CM})$ and $\mathrm{Im}(f_{CM})$ in combination determine the average cell radial velocity.

Equation 5 can be used to further interpret the data of voltage dependence of cell radial velocity shown in Fig. 6 *B*. We will use the cell in a suspending medium of conductivity 56 mS/m as an example for discussion. At an applied voltage of 0.25 V, the cell was levitated to 11 μm above the electrode plane, but it did not move in the radial direction and was trapped over an electrode gap by the radial component of the cDEP force, even though a small unidirectional twDEP force was present. By increasing the applied voltage to 0.3 V, the cell was levitated to a higher position of 15 μm, where the influence of the trapping cDEP force in the radial direction could no longer overcome the twDEP forces. The cell was then no longer trapped and moved in the radial direction under the influence of twDEP forces. Increasing the voltage further resulted in a larger cell velocity. Based on Eq. 5, the time-averaged cell velocity can be written in terms of the applied voltage U as

$$\langle V_r\rangle = \frac{\varepsilon_m r^2 U^2}{3\eta}\mathrm{Im}(f_{CM})F_0(z), \quad (6)$$

where the cDEP force term has been neglected. The factor $F_0(z)$ corresponds to $(E_{x0}^2\nabla\varphi_x + E_{y0}^2\nabla\varphi_y + E_{z0}^2\nabla\varphi_z)\cdot\vec{a}_r$ for a unit applied voltage and decreases with the height z for $z > 10$ μm (Fig. 7 *B*). Equations 6 and 3b indicate that increasing the voltage U will result in two competing effects on the cell radial velocity. The first is to increase $\langle V_r\rangle$ according to the U^2 dependency of Eq. 6, and the second is to lower $\langle V_r\rangle$ through the decrease in $F_0(z)$ resulting from greater levitation of the cell according to Eq. 3b. The combination of these two effects resulted in a net increase in the cell radial velocity with applied voltage, as shown in Fig. 6 *B*, but at a rate slower than a voltage-squared dependency.

Electrode polarization effects

In the low frequency range (below 20 kHz for a suspension conductivity of 56 mS/m, as in Fig. 5 *B*), cell levitation height increased monotonically with frequency. The factor $\mathrm{Re}(f_{CM})$ attained a near-constant value of -0.5 in this frequency range because of the nonconductive cytoplasmic membrane. Thus according to Eq. 3, the frequency dependency of cell height observed here suggests that the parameter $\nabla E_0^2 \cdot \vec{a}_z$ attains the same value at higher positions for higher applied frequencies. This frequency-dependent field distribution effect appears to be a direct result of electrode polarization. The equivalent circuit for the electrode system is shown in Fig. 8. Clearly, the voltage applied to the bulk solution is smaller than that applied to the electrodes because of the voltage drop across the electrode polarization impedance. To determine the voltage applied to the bulk solution, we measured the impedance of the whole electrode system as a function of the field frequency and fit the data to several mathematical models of polarization impedance. The first model, developed by Warburg based on diffusion

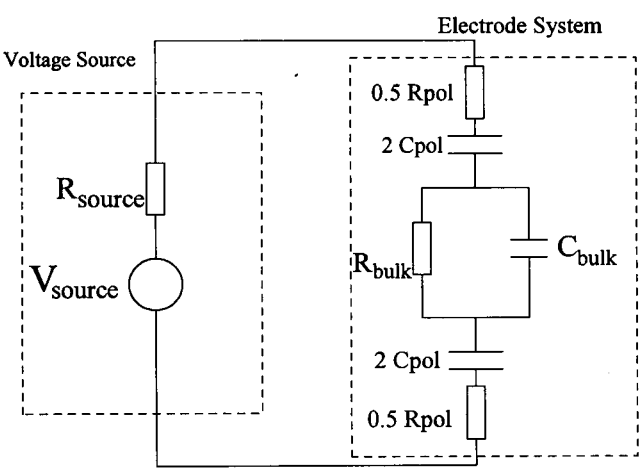

FIGURE 8 Equivalent circuits for the electrode system in which the electrode polarization is characterized by the polarization capacitance (C_{pol}) and resistance (R_{pol}). The total polarization impedance is given by ($R_{pol} - j/(\omega C_{pol})$). The impedance of the bulk solution is represented by the bulk capacitance (C_{bulk}) and resistance (R_{bulk}).

considerations (Schwan, 1992), states that the polarization capacitance and resistance are both proportional to $f^{-0.5}$ and that the impedance has a frequency-independent phase angle of 45°. Other models included various modifications of the Debye-dispersion equation for the polarization impedance, adopted by Jaron et al. (1968) and Buck (1992). Perhaps surprisingly, the relative difference for the frequency-dependent polarization impedances derived with these different models was less than 15% for the frequency range investigated, indicating an inherent consistency between these models under our conditions. Thus, both the bulk solution and the frequency-dependent polarization impedances were deduced, and the true voltage applied to the bulk solution could be calculated. The ratio of the voltage applied to the bulk solution to that on the electrodes is shown in Fig. 9, and it is apparent that for a suspension conductivity of 56 mS/m and a frequency of 1 kHz, the voltage applied to the bulk solution was only about 30% of that on the electrodes.

We have taken into account the electrode polarization effect in our theoretical analysis of both cell levitation height and radial velocity. As shown in Fig. 5 *A*, the experimentally determined frequency dependency of cell height in the low frequency range can be fit reasonably well by the theoretical calculations.

Frequency-dependent cell electrokinetics

To further understand the cell kinetic response shown in Fig. 5, we attempted to fit the measured frequency dependencies of cell height and radial velocity to a theoretical model. The cells were modeled using the so-called single-shell dielectric approximation (Irimajiri et al., 1979; Huang et al., 1995). Because of the limited number of experimental points, we have fitted only two dielectric parameters, namely the membrane capacitance and conductance. The theoretical levitation height and radial velocity are determined from the modeled frequency dependencies of the factors $\mathrm{Re}(f_{CM})$ and $\mathrm{Im}(f_{CM})$ and the field distributions in Fig. 7, *A* and *B*. For clarity, we shall focus on the particular cell in a suspension conductivity of 56 mS/m shown in Fig. 5 *B*, for which the frequency dependencies of $\mathrm{Re}(f_{CM})$ and $\mathrm{Im}(f_{CM})$ are shown in Fig. 10.

In the frequency range of 0.1–10 kHz, $\mathrm{Re}(f_{CM})$ remained almost constant at ~ -0.5. Yet the cell levitation height increased steadily with frequency as a result of the electrode polarization effects discussed above. Theoretically, the cell should have exhibited little or no antifield motion in this range because of small positive values of $\mathrm{Im}(f_{CM})$. However, in experiments it clearly exhibited a small cofield radial motion. Such cofield motion appeared not to be caused by dielectrophoretic forces acting on the cell, but instead was a result of field-induced fluid motion (electroconvection). This assertion is supported by the observation that when polystyrene latex particles of different sizes were subjected to similar electrical field conditions, they exhibited velocities similar to those of the cells in this frequency range. In addition, cells and latex particles did not exhibit rotation during their cofield radial motion. Had this cofield radial motion been caused by twDEP forces relating to an out-of-phase component of the induced cell polarization (reflected by a nonzero, negative $\mathrm{Im}(f_{CM})$), this component would have interacted with the rotating field over the spiral electrode array to result in particle rotation. Reversing the phase sequence of the voltage signals applied to the electrode elements reversed the direction of both particle and cell motion. The nature of such electroconvection remains unclear, although there are reports in the literature (Melcher, 1966; Müller et al., 1993) showing that inhomogeneity in the physical properties of the suspending medium can interact with a traveling field and result in fluid motion. However, the characteristic frequency observed for such effects (e.g., see Müller et al., 1993) was at least two orders

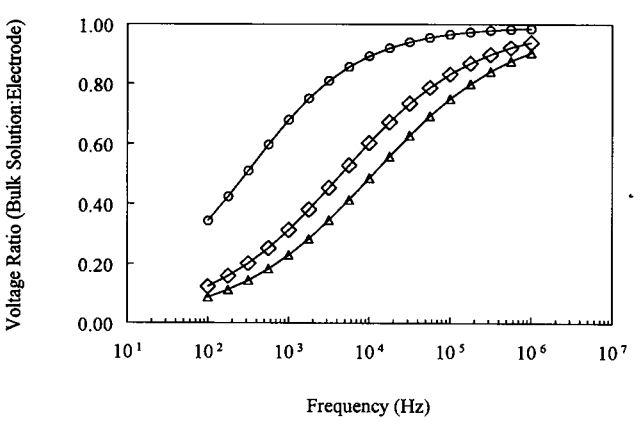

FIGURE 9 The frequency dependency of the proportion of the applied electrical voltage appearing across the bulk solution for suspension conductivities of 18 (○), 56 (◇), and 160 (△) mS/m, calculated according to the model (Schwan, 1992), which assumes that both the polarization capacitance and resistance follow an $f^{-0.5}$ dependence.

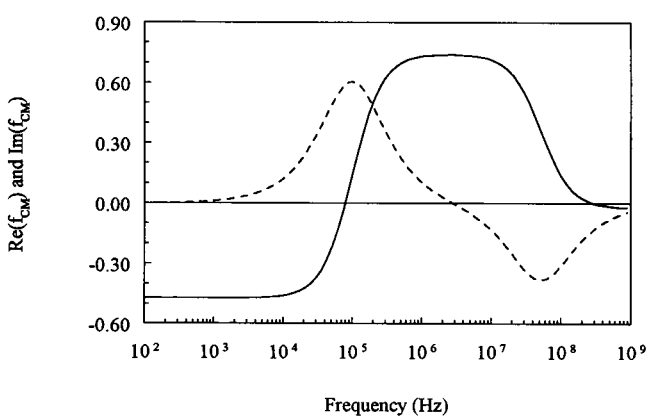

FIGURE 10 The frequency dependency of the real ($\mathrm{Re}(f_{CM})$, ——) and imaginary ($\mathrm{Im}(f_{CM})$, – – –) parts of the Clausius-Mossotti factor calculated for the cell shown in Fig. 5 for a suspension medium of conductivity 56 mS/m. For this simulation, the following parameters were used: cell radius = 6.93 μm, membrane specific capacitance = 22 mF/m^2 and conductance = 320 S/m^2, cell interior conductivity = 0.7 S/m, and permittivity = 75 ϵ_o, where ϵ_o is the dielectric permittivity in free space.

of magnitude higher than that at which apparently electrohydrodynamic effects were observed here.

When the frequency was increased above 10 kHz, $\mathrm{Re}(f_{CM})$ remained negative and gradually reduced in magnitude to zero at ~80 kHz, whereas $\mathrm{Im}(f_{CM})$ increased steadily in magnitude. The cell was levitated to lower equilibrium positions (Eq. 3) in the frequency range of 20–60 kHz as a result of this decrement in $\mathrm{Re}(f_{CM})$. Simultaneously, its radial velocity increased sharply (Eq. 6), not only because of the increment of $\mathrm{Im}(f_{CM})$, but also because the cell experienced a larger traveling field component at lower levitation heights (Fig. 7, *A* and *B*).

In the narrow frequency band between 65 and 75 kHz, $\mathrm{Re}(f_{CM})$ was negative but close to zero, whereas $\mathrm{Im}(f_{CM})$ exhibited large positive values (>0.5). Because $\mathrm{Re}(f_{CM})$ was small, the cell was levitated to a small height (~10 μm above the electrode plane), where the radial components of cDEP and twDEP forces acting together trapped the cell over an electrode edge. Thus cell movement across more than one electrode width/gap period was no longer possible. When the frequency was increased further to ~120 kHz, $\mathrm{Re}(f_{CM})$ became positive but was of small magnitude (<0.2), and the cell was no longer levitated, but instead rested at heights where the phase-nonuniformity factor reversed its radial direction. This resulted in a twDEP force that induced cofield movement. When the frequency was increased still further, so that the magnitude of $\mathrm{Re}(f_{CM})$ increased above 0.2, the resulting positive cDEP forces were sufficiently large to overcome the twDEP force influence and the cell was trapped at the electrode edges. In this case, the unidirectional twDEP force component determined the electrode edge at which the cell was trapped. For example, under an inward-phase excitation, the cell was trapped at the outward-facing electrode edges. Overall, in this frequency range, where the factor $\mathrm{Re}(f_{CM})$ changed sign, the cell kinetic response was critically sensitive to frequency, as confirmed by the theoretical simulations of the frequency dependency of the DEP forces acting on the cell. However, the theoretical simulation predicted an even narrower frequency region for this cell kinetic transition. This discrepancy between theory and experiment may have arisen from, among other factors, the neglect in the simulation of higher-order DEP forces (Washizu and Jones, 1996) and the influence of the cell on the local electrical field distribution, factors that could become significant when a cell is close to an electrode surface. Because an inherent heterogeneity in cell dielectric properties existed within the bulk cell population, different cells exhibited values of $\mathrm{Re}(f_{CM})$ that ranged through both positive and negative values at a given field frequency in the cDEP cross-over region. As a result, different cells showed a variety of cell kinetic responses in this transition-frequency band.

Increasing the frequency above the transition region resulted in further increments in $\mathrm{Re}(f_{CM})$. cDEP forces then became so large that the cell kinetic behavior was dominated by $\mathrm{Re}(f_{CM})$ and the cell was pulled to, and trapped at, the closest edge of the electrode elements. Finally, in the high-frequency range of 50–100 MHz, $\mathrm{Re}(f_{CM})$ approached zero, and whether cells were trapped on the inward-facing or outward-facing edge of the electrode elements again depended sensitively on the phase sequence of the applied voltage signals.

Applications of spiral electrode arrays

As in the case of several previously reported electrode geometries (Huang et al., 1993; Fuhr et al., 1995; Talary et al., 1996), a spiral array under phase-quadrature excitation is capable of exerting both cDEP and twDEP forces on cells as a result of the in-phase ($\mathrm{Re}(f_{CM})$) and out-of-phase ($\mathrm{Im}(f_{CM})$) components of field-induced polarization interacting, respectively, with the field inhomogeneities in magnitude and phase distributions. Despite this common feature, this is the first time cell electrokinetic responses (including entrapment, levitation, and radial motion) have been quantitatively analyzed in terms of cDEP and twDEP forces simulated using a generalized DEP theory (Wang et al., 1995). Thus we are able to show that cDEP forces either trap cells on electrode edges or levitate them above the electrode plane, depending on whether $\mathrm{Re}(f_{CM})$ is positive or negative. Our analysis also reveals that when cells are levitated, the twDEP forces that give rise to their radial motion are height dependent and therefore depend not only on $\mathrm{Im}(f_{CM})$, but also on $\mathrm{Re}(f_{CM})$.

Our spiral array bears similarities to the meandering ("squared spiral") electrode structure of Fuhr and his coworkers (Fuhr et al., 1995; Müller et al., 1996). Nevertheless, the operational principle used in the study by Müller et al. (1996), in which electrodes were energized to generate only cDEP forces for particle trapping, is quite different from our combined cDEP and twDEP approach. Fuhr et al. (1995) used a meandering electrode that was masked, except in two intersecting channel regions. By energizing that system with phase-quadrature signals, two linear, intersecting TWD devices were produced. We note, however, that twDEP-induced linear velocities may depend on cell locations in that case, because different DEP forces are expected for positions at different distances from the 90° turning corners, and for positions at different distances from the edges of the coverglass plates. The glass plates used to mask the electrode and to give linear traveling-electrode channels also resulted in a smaller active area for cell manipulation compared with that of a spiral array of similar size.

Like the meandering electrode structure, the active area of a spiral array for cell manipulation can be readily extended to cover a larger region of space while maintaining the need for only four electrode connections. This contrasts sharply with linear traveling electrode arrays in which either complex electrode wiring (Huang et al., 1993) or a multilayer fabrication technique must be introduced to produce a large array (Fuhr et al., 1995; Talary et al., 1996). Thus large linear arrays are much more expensive to realize than spiral electrode systems.

By utilizing both cDEP and twDEP forces simultaneously for cell manipulation, the spiral electrode array offers several advantages over electrode devices using cDEP forces alone. First, cDEP forces are proportional to the inhomogeneity in the electrical field strength. Except in the so-called isomotive electrode design (Pethig, 1979), field inhomogeneity varies spatially, so that cDEP forces acting on cells depend strongly on cell position (Wang et al., 1993). This limits the discriminatory ability for selective cDEP manipulation of cells. In the spiral array used here, the cDEP-induced levitation and the twDEP-induced radial velocity are almost independent of cell location on the electrodes, and cell differential heights and velocities depend solely on heterogeneity in the cell dielectric characteristics. In addition, cell radial velocities in a spiral array are governed by both $\mathrm{Re}(f_{CM})$ and $\mathrm{Im}(f_{CM})$, and this dependency on dual, independent parameters promises highly selective cell manipulation compared with cDEP manipulation, which depends on $\mathrm{Re}(f_{CM})$ alone.

Second, microelectrode arrays such as polynomial electrodes (Huang and Pethig, 1991) and others (Fuhr et al., 1992) have been shown to be capable of concentrating cells at isolated electric field minima by negative cDEP. However, cDEP forces generated by these electrodes are inversely proportional to the characteristic dimension of the active area, and signals of large magnitude would be needed for cell collection on a relative large region. For example, for a $n = 2$ polynomial electrode array (Huang and Pethig, 1991), an applied voltage of 3.5 V RMS was required to concentrate cells from an area of 0.4 mm^2. As the active area is increased, the need for a higher voltage increases and this creates a fundamental limitation in the maximum design size for cell manipulation because of the damage that high field strengths at positions close to electrode edges can do to living cells. In a spiral array, for a comparable active area of 0.4 mm^2, applied voltages of only 0.7 V RMS were needed to concentrate cells (Fig. 10). Similar results using the same field strengths were achieved for a spiral area of 6.4 mm^2 (data not shown). DEP forces here are independent of the array size and depend only on the width and spacing of the periodic spiral electrode elements. Although cDEP periodic arrays such as interdigitated, castellated electrodes (Pethig et al., 1992) are effective in generating field inhomogeneities over a large area (6 cm^2), these trap cells at many locations distributed in a pattern over the entire array area. Therefore they cannot selectively concentrate cells of specific type(s) in a mixture and bring them to a single target location. Consequently, they are of limited value in isolating rare cell types from a cell mixture.

Third, cell cDEP behavior is determined by the electric field distribution, and this is fixed by the particular electrode geometry. Therefore little or no control can be exerted over cell spatial responses by changing the applied electrical signals. In contrast to this, the cell kinetic responses on a spiral array can be readily altered by varying the phase sequences and frequency of the voltage signals.

Finally, although cDEP separations of cells have been demonstrated for mixtures of cells having large dielectric differences, such as viable and nonviable cells, or cells having enormous morphological differences (e.g., Becker et al., 1995; Markx and Pethig, 1995), cell-cell electrical interactions (Wang et al., 1994) tend to attract cells, and these may strongly affect the discriminatory ability during cell separation. For example, even in the cDEP separation of breast cancer cells from blood, for which the cells had relatively large dielectric differences (Becker et al., 1995), a swept-frequency protocol had to be designed to release blood cells trapped within masses of tumor cells by cell-cell interactions. The combined use of cDEP and twDEP forces in the spiral electrode system appears to significantly reduce the problem of cell-cell interactions.

Some applications of the spiral electrodes include:

1. Cell concentration. For some biomedical applications, concentrating cells from a dilute suspension to a target location is necessary. One could concentrate bacteria from urine using the spiral electrode and exploit differences in the dielectric properties of Gram-positive and Gram-negative bacteria (Markx et al., 1994) to discriminate between them. As an example of such cell concentration, Fig. 11 shows the concentration of MDA-MB-231 cells at the center of the spiral array.

2. Cell isolation and detection. In this case, the sample would contain a mixture of cells in which only one or a few specific types are required to be concentrated. For example, the isolation of highly dispersed tumor cells from normal cell mixtures such as blood and bone marrow is critical for cancer diagnosis and treatment. The application criteria are that at one specific frequency (or range) one cell type exhibits entrapment behavior and the others are caused to move to the center or the peripheral regions. Using this approach, we have successfully isolated MDA-MB-231 cells from mixtures with blood (data to be published later).

CONCLUSIONS

The spiral electrode configuration reported here has been characterized through experimental observations of cell kinetics and theoretical analysis of the DEP forces acting on cells. Depending on the frequency and phase sequence of applied voltages, spiral electrodes exert forces in three dimensions, resulting in cell radial motion, levitation, and trapping. The observed voltage and frequency dependencies of these phenomena can be readily interpreted through knowledge of the generalized DEP force equation, the cell dielectric properties, the field distribution, and the electrode polarization impedance.

Spiral electrode arrays offer many potential applications in biomedicine, including cell separation, filtering, isolation, and concentration. Special attention is required to address the electroconvection and electrode polarization effects observed in the lower frequency range. Furthermore, the possibility of applying signals of multiple frequency

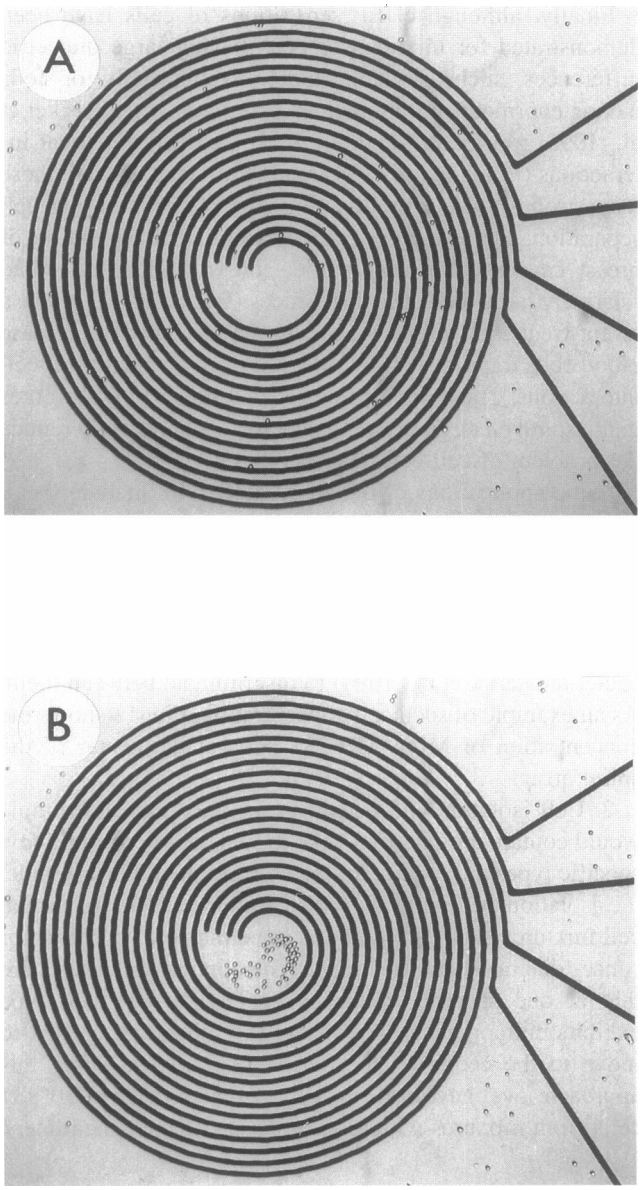

FIGURE 11 (*A*) MDA-MB-231 cells randomly distributed on a spiral electrode array before the application of voltage signals. (*B*) Twenty seconds after the application of voltage signals of 50 kHz and 0.7 V (RMS) and outward phase sequence, the cells were collected at the central region of the spiral electrode array.

components to generate more flexible DEP manipulation forces should be investigated. In addition, the chamber containing electrode structures on both the top and bottom walls should be studied, to test a more uniform radial twDEP force distribution. Finally, studies should be carried out to determine the optimum ratio of cell size to electrode and gap dimensions.

We thank Jamileh Noshari and Carrie Hamilton for cell culture work and Giovanni De Gasperis, Jun Yang, and Jody Vykoukal for valuable discussions.

This work is supported in part by a Biomedical Engineering Research grant from the Whitaker Foundation and a Development Fund from a Cancer Center Support grant (CA16672) from the National Institutes of Health.

REFERENCES

Becker, F. F., X.-B. Wang, Y. Huang, R. Pethig, J. Vykoukal, and P. R. C. Gascoyne. 1994. The removal of human leukaemia cells from blood using interdigitated microelectrodes. *J. Phys. D Appl. Phys.* 27: 659–2662.

Becker, F. F., X.-B. Wang, Y. Huang, R. Pethig, J. Vykoukal, and P. R. C. Gascoyne. 1995. Separation of human breast cancer cells from blood by differential dielectric affinity. *Proc. Natl. Acad. Sci. USA.* 29:860–864.

Bertoncello, I., T. R. Bradley, and S. Z. Watt. 1991. An improved negative immunomagnetic selection strategy for the purification of primitive hemopoietic cells from normal bone marrow. *Exp. Hematol.* 19:95–100.

Buck, R. P. 1992. Impedances of thin and layered systems: cells with even or odd numbers of interfaces. *Ann. Biomed. Eng.* 20:363–383.

Cailleau, R., M. Olive, and Q. V. J. Cruciger. 1978. Long-term human breast carcinoma cell lines of metastatic origin: preliminary characterization. *In Vitro* 14:911–915.

Chan, W. C., G. Q. Wu, T. C. Greiner, J. M. Vose, and J. G. Sharp. 1994. Detection of tumor contamination of peripheral stem cells in patients with lymphoma using cell culture and polymerase chain reaction technology. *J. Hematother.* 3:175–184.

Craig, J. I. O., K. Langlands, A. C. Parker, and R. S. Anthony. 1992. Molecular detection of tumor contamination in peripheral blood stem cell harvests. *Exp. Hematol.* 22:898–902.

Fuhr, G., W.-M. Arnold, R. Hagedorn, T. Müller, W. Benecke, B. Wagner, and U. Zimmermann. 1992. Levitation, holding and rotation of cells within traps made by high-frequency fields. *Biochim. Biophys. Acta.* 1108:215–233.

Fuhr, G., T. Schnelle, T. Müller, H. Glasser, T. Lisec, and B. Wagner. 1995. Positioning and manipulation of cells and microparticles using miniaturized electric field traps and travelling waves. *Sensors Mater.* 7:131–146.

Gascoyne, P. R. C., Y. Huang, R. Pethig, J. Vykoukal, and F. F. Becker. 1992. Dielectrophoretic separation of mammalian cells studied by computerized image analysis. *Meas. Sci. Technol.* 3:439–445.

Gross, H.-J., B. Verwer, D. Houck, R. A. Hoffman, and D. Recktenwald. 1995. Model study detecting breast cancer cells in peripheral blood mononuclear cells at frequencies as low as 10^{-7}. *Proc. Natl. Acad. Sci. USA.* 92:537–541.

Hölzel, R. 1993. A simple wide-band sine wave quadrature oscillator. *IEEE Trans. Instrum. Meas.* 42:758–760.

Huang, Y., and R. Pethig. 1991. Electrode design for negative dielectrophoresis. *Meas. Sci. Technol* 2:1142–1146.

Huang, Y., R. Pethig, R. Hölzel, and X.-B. Wang. 1992. Differences in the A. C. electrodynamics of viable and non-viable yeast cells determined through combined dielectrophporesis and electrorotation studies. *Phys. Med. Biol.* 37:1499–1517.

Huang, Y., X.-B. Wang, F. F. Becker, and P. R. C. Gascoyne. 1995. Electrorotational studies of the cytoplasmic dielectric properties of Friend murine erythroleukaemia cells. *Phys. Med. Biol.* 40:1789–1806.

Huang, Y., X.-B. Wang, J. Tame, and R. Pethig. 1993. Electrokinetic behaviour of colloidal particles in travelling electric fields: studied using yeast cells. *J. Phys. D Appl. Phys.* 26:1528–1535.

Hughes, M. P., R. Pethig, and X.-B. Wang 1996. Dielectrophoretic forces on particles in travelling electric fields *J. Phys. D Appl. Phys.* 29: 474–482.

Irimajiri, A., T. Hanai, and A. Inouye. 1979 A dielectric theory of "multistratified shell" model with its application to a lymphoma cell. *J. Theor. Biol.* 78:251–269.

Jaron, D., H. P. Schwan, and D. B. Geselowitz. 1968. A mathematical model for the polarization impedance of cardiac pacemaker electrodes. *Med. Biol. Eng.* 6:579–594.

Kaler, K. V. I. S., and T. B. Jones. 1990. Dielectrophoretic spectra of single cells determined by feedback-controlled levitation. *Biophys. J.* 57: 173–182.

Kaler, K. V. I. S., J. Xie, T. B. Jones, and R. Paul. 1992. Dual-frequency dielectrophoretic levitation of Canola protoplasts. *Biophys. J.* 63:58–69.

Kuo, S. C., and M. P. Sheetz. 1993. Force of single kinesin molecules measured with optical tweezers. *Science.* 260:232–234.

Markx, G. H., Y. Huang, X.-F. Zhou, and R. Pethig. 1994. Dielectrophoretic characterization and separation of micro-organisms. *Microbiology.* 140:585–591.

Markx, G. H., and R. Pethig. 1995. Dielectrophoretic separation of cells: continuous separation. *Biotechnol. Bioeng.* 45:337–343.

Masuda, S., M. Washizu, and M. Iwadare. 1987. Separation of small particles suspended in liquid by nonuniform traveling field. *IEEE Trans. Ind. Appl.* 23:474–480.

Melcher, J. R. 1966. Traveling-wave induced electroconvection. *Phys. Fluids.* 9:1548–1555

Müller, T., W. M. Arnold, T. Schnelle, R. Hagedorn, G. Fuhr, and U. Zimmermann. 1993. A traveling-wave micropump for aqueous solutions: comparison of 1 g and μg results. *Electrophoresis.* 14: 764–772.

Müller, T., A. Gerardino, T. Schnelle, S. G. Shirley, F. Bordoni, G. De Gasperis, R. Leoni, and G. Fuhr. 1996. Trapping of micrometre and sub-micrometre particles by high-frequency electric fields and hydrodynamic forces. *J. Phys. D: Appl. Phys.* 29:340–349.

Ormerod, M. G. 1994. Flow Cytometry: A Practical Approach, 2nd Ed. IRL Press at Oxford University Press, Oxford.

Pethig, R. 1979. Dielectric and Electronic Properties of Biological Materials, ch 6. Wiley, Chichester. 186–206.

Pethig, R., Y. Huang, X.-B. Wang, and J. P. H. Burt. 1992. Positive and negative dielectrophoretic collection of colloidal particles using interdigitated castellated microelectrodes. *J. Phys. D Appl. Phys.* 24: 881–888.

Schwan, H. P. 1992. Linear and nonlinear electrode polarization and biological materials. *Ann. Biomed. Eng.* 20:269–288.

Talary, M. S., J. P. H. Burt, J. A. Tame, and R. Pethig. 1996. Electromanipulation and separation of cells using traveling electric fields. *J. Phys. D Appl. Phys.* 29:2198–2203.

Talary, M. S., K. I. Mills, T. Hoy, A. K. Burnett, and R. Pethig. 1995. Dielectrophoretic separation and enrichment of CD34+ cell subpopulation from bone marrow and peripheral blood stem cells. *Med. Biol. Eng. Comput.* 33:235–237.

Wang, X., X.-B. Wang, F. F. Becker, and P. R. C. Gascoyne. 1996. A theoretical method of electrical field analysis for dielectrophoretic electrode arrays using Green's theorem. *J. Phys. D: Appl. Phys.* 29: 1649–1660.

Wang, X.-B., Y. Huang, J. P. H. Burt, G. H. Markx, and R. Pethig. 1993. Selective dielectrophoretic confinement of bioparticles in potential energy wells. *J. Phys. D Appl. Phys.* 26:1278–1285.

Wang, X.-B., Y. Huang, P. R. C. Gascoyne, and F. F. Becker. 1994. Particle dipole-dipole interaction in AC electric fields. *Proc. 16th Int. Conf. IEEE/EMBS* 2:774–775.

Wang, X.-B., M. P. Hughes, Y. Huang, F. F. Becker, and P. R. C. Gascoyne. 1995. Non-uniform spatial distributions of both the magnitude and phase of AC electric fields determine dielectrophoretic forces. *Biochim. Biophys. Acta.* 1243:185–194.

Washizu, M., and T. B. Jones. 1996. Generalized multipolar dielectrophoretic force and electrorotational torque calculation. *J. Electrostat.* 37:121–134.

Washizu, M., T. B. Jones, and K. V. I. S. Kaler. 1996. Higher-order dielectrophoretic effects: levitation at a field null. *Biochim. Biophys. Acta.* 1158:40–46.

Zhang, R. D., I. J. Fidler, and J. E. Price. 1991. Relative malignant potential of human breast carcinoma cell lines established from pleural effusions and a brain metastasis. *Invasion Metastasis.* 11:204–215.